3 RESULTS AND DISCUSSION

3.1 Syntheses of ligand and complexes

The 4-methyl-2-(phenylazo)pyridine (4mazpy) ligand was synthesized by the condensation of the 2-amino-4-methylpyridine and the nitrosobenzene in 1:1 mole ratio in the mixture of sodium hydroxide and benzene solution. The reaction was refluxed for 15 h. Then, the mixture was extracted with benzene and purified by column chromatography. The red-orange product was isolated. The reaction is shown in equation (1).

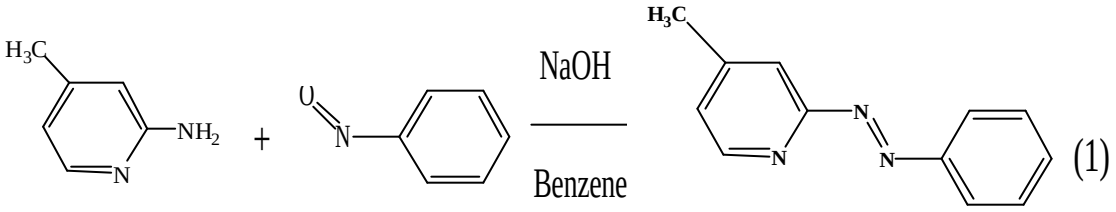

(1)

2-amino-4-methylpyridine nitrosobenzene 4-methyl-2-(phenylazo)pyridine (4mazpy)

The yield of 4-methyl-2-(phenylazo)pyridine was 61 %. The physical properties of the 4mazpy ligand are listed in Table 1.

Table 1. The physical properties of 4mazpy

Ligand	Physical properties		
	Appearance	Color	Melting point (?C)
4mazpy	Solid	Red-orange	48-50

The melting point of the 4mazpy ligand was in the range 48-50 ?C. The red-orange ligand was the solid state. The solubility of 10 mg of ligand was tested in 5 mL of various solvents. The ligand was very soluble in almost all solvents.

The 4-methyl-2-(phenylazo)pyridine (4mazpy) ligand is a bidentate ligand containing the azoimine functional group, -N=N-C=N-, which has N-N donor atoms. Reaction of 4mazpy with $RuCl_3.3H_2O$ in ethanol produced the complexes of $[Ru(4mazpy)_2Cl_2]$ via spontaneous reductive chelation. The complexes were isolated in high yield from the reaction mixture. The reactions afforded three isomers. They were *ctc*, *ccc* and *tcc*-$[Ru(4mazpy)_2Cl_2]$ complexes. The coordination number of these complexes was six- coordinated. The physical properties of the complexes are summarized in Table 2.

Table 2. The physical properties of the $[Ru(4mazpy)_2Cl_2]$ complexes

compound	Physical properties		
	Appearance	Color	Melting point (?C)
ctc-$[Ru(4mazpy)_2Cl_2]$	Solid	blue	325-326
ccc$[Ru(4mazpy)_2Cl_2]$	Solid	purple	330-331
tcc-$[Ru(4mazpy)_2Cl_2]$	Solid	green	335-336

The solubility of 10 mg of the $[Ru(4mazpy)_2Cl_2]$ complexes was tested in 10 mL of various solvents. The results showed that complexes were slightly soluble in MeOH, EtOH, toluene, and acetone. It was completely soluble in dichloromethane, chloroform and acetonitrile but insoluble in ether and water.

3.2 Characterization of ligand and complexes

The chemistry of the 4mazpy ligand and complexes was determined by using these techniques.

3.2.1 Elemental analysis
3.2.2 Fast-atom bombardment (FAB) mass spectrometry
3.2.3 Infrared spectroscopy
3.2.4 UV-Visible absorption spectroscopy
3.2.5 Nuclear Magnetic Resonance spectroscopy (1D and 2D)
3.2.6 Cyclic Voltammetry
3.2.7 X-ray Crystallography

3.2.1 Elemental analysis

Elemental analysis is a technique to study the composition of elements in a compound. It is shown that the analytical data of the compounds corresponded to the calculated values. The elemental analysis data are listed in Table 3.

Table 3. Elemental analysis data of the 4mazpy ligand and the $[Ru(4mazpy)_2Cl_2]$ complexes

compounds	% C		% H		% N	
	Calc.	Found	Calc.	Found	Calc.	Found
4mazpy	73.08	72.85	5.62	5.65	21.30	22.61
ctc-$[Ru(4mazpy)_2Cl_2]$	50.89	50.65	3.91	3.76	14.84	15.35
ccc-$[Ru(4mazpy)_2Cl_2]$	50.89	50.36	3.91	3.72	14.84	14.15
tcc-$[Ru(4mazpy)_2Cl_2]$	50.89	49.49	3.91	3.84	14.84	14.98

3.2.2 Fast-atom bombardment (FAB) mass spectrometry

The FAB mass spectrometry is a technique to study the molecular mass of compound.

The FAB mass spectrum of the 4mazpy ligand is shown in Figure 4. From the data, the maximum peak, which gave 35% relative abundance at m/z 198, corresponded to the molecular weight of the ligand and the 100% relative abundance at 76 was the $[phenyl\text{-}H]^+$.

All three $[Ru(4mazpy)_2Cl_2]$ complexes showed the peak at m/z 566, and 551 which were assigned to the $[Ru(4mazpy)_2Cl_2]]^+$ and the $[Ru(4mazpy)_2Cl_2]\text{-}CH_3]^+$, respectively. The FAB mass spectra are shown in Figure 5 to Figure 7.

This method confirmed the expected formula and molecular mass of the ligand and the complexes. The results from this technique are summarized in the Table 4.

Table 4. FAB mass spectroscopic data of 4mazpy and $[Ru(4mazpy)_2Cl_2]$

Compounds	m/z	Stoichiometry	Equivalent species	Rel. Abun. (%)
4mazpy	198	$[4mazpy+H]^+$	$[L+H]^+$	35
	76	$[phenyl\text{-}H]^+$	$[phenyl\text{-}H]^+$	100
ctc-$[Ru(4mazpy)_2Cl_2]$	551	$[Ru(L)_2Cl_2]\text{-}CH_3]^+$	$[M\text{-}CH_3]^+$	60
	566	$[Ru(L)_2Cl_2]]^+$	$[M]^+$	20
ccc-$[Ru(4mazpy)_2Cl_2]$	550	$[Ru(L)_2Cl_2]\text{-}CH_3\text{-}H]^+$	$[M\text{-}CH_3\text{-}H]^+$	35
tcc-$[Ru(4mazpy)_2Cl_2]$	550	$[Ru(L)_2Cl_2]\text{-}CH_3\text{-}H]^+$	$[M\text{-}CH_3\text{-}H]^+$	40
	566	$[Ru(L)_2Cl_2]^+$	$[M]^+$	20
	248	$[Ru(L)_2Cl_2]\text{-}2Cl]^+$	$[M\text{-}2Cl]^+$	100

MW. of 4mazpy (L) = 197.21 g/mol, MW. of $[Ru(4mazpy)_2Cl_2]$ (M) = 566.45 g/mol

3.2.3 Infrared spectroscopy

Infrared spectroscopy is a technique to study the functional groups of compounds. Infrared spectra were collected by using KBr pellets in the range 4000-370 cm^{-1}. The important vibrational frequencies are C=C, C=N, N=N (azo) stretching modes and C-H bending in monosubstituted benzene.

Infrared spectroscopy of the 4mazpy ligand

The infrared spectroscopic data of the 4mazpy ligand are listed in Table5.

Table 5. Infrared spectroscopic data of the 4mazpy ligand

Vibration modes	Frequencies (cm^{-1})
C=C, C=N stretching	1598 (s) 1489 (m) 1471 (m) 1445 (m)
N=N stretching	1383 (s)
C-H bending in monosubstituted benzene	835 (s) 773 (s) 686 (s)

s = strong, m = medium

The infrared spectrum of 4mazpy exhibited intense bands at 1600-370 cm^{-1}. The ligand showed medium peaks at 1598-1445 cm^{-1}, corresponding to C=C and C=N

stretching in the pyridine ring of the ligand. The sharp band at 1383 cm^{-1} was assigned to the N=N stretchings, which was had a lower frequency than that in azpy (1421 cm^{-1}) (Changsaluk, U., 2003). This stretching mode was used to be considered the ?-acid property in azo complexes. It was found that the N=N bond of the free azpy ligand is stronger than that of 4mazpy ligands. In addition, this vibrational band is expected to be of higher frequency than that in the complexes due to the coordination of ligand to ruthenium metal. The infrared spectrum is shown in Figure 8.

Infrared spectroscopy of the $[Ru(4mazpy)_2Cl_2]$ complexes

The infrared spectroscopic data of the complexes are listed in Table 6.

Table 6. Infrared spectroscopic data of $[Ru(4mazpy)_2Cl_2]$ complexes

Vibration modes	Frequencies (cm^{-1})		
	ctc-$[Ru(L)_2Cl_2]$	*ccc*-$[Ru(L)_2Cl_2]$	*tcc*-$[Ru(L)_2Cl_2]$
C=C, C=N stretching	1614 (m) 1452 (m)	1615 (m) 1453 (m)	1615 (m) 1475 (m) 1454 (m)
N=N stretching	1318 (s) 1245 (s)	1303 (s) 1245 (s)	1305 (s) 1243 (s)
C-H bending in monosubstituted benzene	834 (m) 765 (m) 699 (m)	828 (m) 765 (m) 697 (m)	820 (m) 763 (m) 698 (m)

s = strong, m = medium

In the complexes, the infrared spectra exhibited medium peaks at 1615-1452 cm^{-1}. These frequencies were assigned to the C=C and the C=N vibrational modes. The ?(N=N) (1303-1318 cm^{-1}) is red shift by 65-80 cm^{-1}, compared to the free ligand value (1383 cm^{-1}) which is a good indication of N-coordination. The N=N stretching frequencies of the ligand and the complexes are summarized in Table 7.

Table 7. The N=N stretching frequencies of the ligand and the complexes

Compounds	N=N stretching (cm^{-1})
4mazpy	1383
ctc-[$Ru(4mazpy)_2Cl_2$]	1318
ccc-[$Ru(4mazpy)_2Cl_2$]	1303
tcc-[$Ru(4mazpy)_2Cl_2$]	1305

The N=N stretching modes in the complexes appeared at lower frequency than that in the free ligand. It was due to the ?-back bonding occurring from the t_{2g} orbitals of metal to the ?* orbitals of azo. From this result, the bond order of N=N (azo) decreased and the bond length increased, so the vibrational energies decreased. In addition, ?(N=N) of the *ctc*-[$Ru(4mazpy)_2Cl_2$] appeared at the higher frequency than the *ccc*- and *tcc*-[$Ru(4mazpy)_2Cl_2$]. It indicated that the 4mazpy in *ctc* could accept electrons from the t_{2g}(Ru) orbitals to its ?* orbitals less than *ccc* and *tcc* (*ccc*, *tcc* > *ctc*). The infrared spectra of the [$Ru(4mazpy)_2Cl_2$] isomers are shown in Figure 9, 10 and 11, respectively.

3.2.4 UV-Visible absorption spectroscopy

UV-Visible absorption spectroscopy is a technique to study the electronic transitions of compound. The electronic absorption spectral of the complexes in five solvents were recorded in the range of 200-800 nm. The spectral data are given in Table 8. The absorption spectra of all compounds in CH_2Cl_2, $CHCl_3$, CH_3CN, DMF and DMSO are shown in Figure 12 to Figure 15.

Table 8. UV-Visible absorption spectroscopic data of the ligand and the complexes

compounds	λ_{max} nm, ($\varepsilon^a \times 10^4$ $M^{-1}cm^{-1}$)				
	CH_2Cl_2	$CHCl_3$	CH_3CN	DMF	DMSO
4mazpy	319(1.6) 451(0.04)	319 (1.7) 450(0.04)	315 (1.3) 443 (0.04)	317 (1.4) 449(0.04)	319(1.5) 449(0.05)
ctc - $[Ru(4mazpy)_2Cl_2]$	319 (2.8) 581 (1.3)	318 (3.3) 588 (1.6)	316 (2.7) 587 (1.3)	318 (2.4) 594 (1.1)	317(3.2) 596(1.5)
ccc -$[Ru(4mazpy)_2Cl_2]$	324 (2.0) 583 (1.2)	325 (1.5) 578 (0.9)	317 (2.1) 574 (1.2)	322 (2.4) 581(1.3)	324(1.6) 578(0.9)
tcc - $[Ru(4mazpy)_2Cl_2]$	292(2.7) 399(0.9) 630(1.3)	301 (1.8) 406 (0.9) 629 (1.3)	300 (2.2) 394 (1.2) 633 (1.5)	300 (2.6) 397 (1.2) 637 (1.5)	305(2.5) 400(1.3) 638(1.7)

[a] Molar extinction coefficient

UV-visible spectral studies of the free ligand displayed absorption at 315-319 nm ($\varepsilon \sim 15000$ $M^{-1}cm^{-1}$) which was assigned to $\pi \rightarrow \pi^*$ transition and the very low intensity band in visible region, 443-451 nm ($\varepsilon \sim 400$ $M^{-1}cm^{-1}$) was assigned

to n? ?* . These bands are due to the intraligand charge transition. Figure 12 shows the UV-Visible absorption spectrum for the 4mazpy ligand in CH_2Cl_2 solvent.

The two *cis* complexes , *ctc*-[Ru(4mazpy)$_2$Cl$_2$] and *ccc*-[Ru(4mazpy)$_2$Cl$_2$] displayed intense bands in UV region within the range 316-325 nm, intraligand charge transfer transition and at 574-596 nm, metal-to-ligand charge-transfer transition. Whereas, the *trans*-[Ru(4mazpy)$_2$Cl$_2$] complex showed one absorption band (? ? 20000 $M^{-1}cm^{-1}$) in the region 292-305 nm which was assigned to intraligand charge transfer transition and two absorption bands (394-406 nm and 629-638 nm) were assigned to the t_2(Ru) ? ?*(L) (MLCT) transitions. The electronic spectra of *cis* complexes in the visible region (574-596 nm) which existed in two isomeric forms appeared at the higher energies than those of the *trans* complex, (629-638 nm). It is interesting to note that the trend in the MLCT band's feature between the *trans* and the *cis* complexes are as follows. The *cis* complexes displayed two different intense band characters. The most intense bands were in the range of 316-325 nm and the less intense bands were in the range of of 574-596 nm. While, the spectrum of the *trans* complex showed two intense bands at the UV region and one band in the visible region which was more intense band than those of the *cis* complexes. These intense bands were believed to be the spin-allowed singlet-singlet transition. Figure 13, 14 and 15 show the UV-Visible absorption spectra for all the three complexes in CH_2Cl_2 solvent.

3.2.5 Nuclear Magnetic Resonance spectroscopy (1D-2D)

Nuclear Magnetic Resonance (NMR) spectroscopy is a technique to determine the molecular structure of a compound. The structures of ligand and complexes were investigated by using 1D and 2D NMR spectroscopic techniques (^{1}H NMR, ^{1}H-^{1}H COSY NMR, ^{13}C NMR, DEPT NMR and ^{1}H-^{13}C HMQC NMR). The NMR spectra of all compounds were recorded in $CDCl_3$ on UNITY SNOVA 500 MHz. The tetramethylsilane ($Si(CH_3)_4$) was used as an internal reference.

Nuclear Magnetic Resonance spectroscopy of the 4-methyl-2-(phenylazo)pyridine ligand

Table 9. ^{1}H and ^{13}C NMR spectroscopic data of the 4mazpy ligand

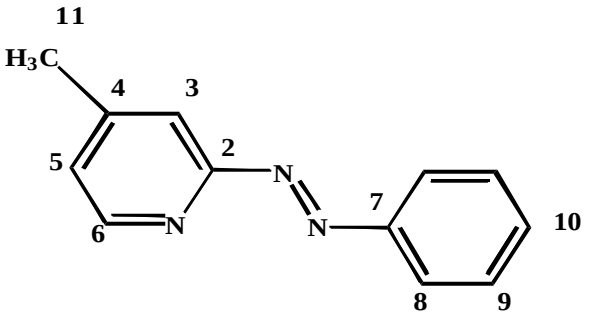

H-position	^{1}H NMR			^{13}C NMR
	? (ppm)	*J* (Hz)	Number of H	*?* (ppm)
6	8.5 (d)	5	1	149
8	8.0 (dd)	8.5, 1.5	2	123
3	7.5 (s)	-	1	116

Table 9. (Continued)

H-position	^{1}H NMR			^{13}C NMR
	? (ppm)	*J* (Hz)	Number of H	? (ppm)
9 10	7.4 (m)	-	3	129 132
5	7.1 (d)	4.5	1	126
11	2.4 (s)	-	3	21
Quaternary carbons				163, C2 152, C7 150, C4

s = singlet, d = doublet, t = triplet, dd = doublet of doublet

The 4-methyl-2-(phenylazo)pyridine (4mazpy) has eleven protons on the molecule. The ^{1}H NMR spectrum of 4mazpy showed six signals (Figure 16). The highest field signal was assigned to H11 (-CH_3) which has the highest intensity. The proton H5 (? = 7.1 ppm) and H6 (? = 8.5 ppm) appeared as a doublet peak by coupling with *J* ortho, 5 Hz. The most downfield of H6 was due to the nitrogen atoms which was located clos to it. The proton H3 occurred as a singlet peak at 7.5 ppm, (s). The signal of proton H9 and H10 showed as multiplet peaks at the same position due to both protons being located close to each other. In the phenyl ring, the proton H8 were two equivalent protons. The signal occurred as a doublet of doublet at 8.05 ppm. This resonance appeared at the lower field than the proton H9 and H10 because it located next to the azo nitrogen, the ^{1}H NMR spectrum of the 4mazpy ligand was shown in Figure 16. In addition, the peak assignment was supported by using simple correlation ^{1}H-^{1}H COSY NMR spectroscopy. The^{1}H-^{1}H COSY NMR signals are presented in Figure 17.

The ^{13}C NMR (Figure 18) results corresponded to those from DEPT NMR (Figure 19), which showed only methine carbon signals. The ^{13}C NMR spectrum of the 4mazpy ligand gave 10 signals for 10 carbons. The quaternary carbon C2 of the pyridine ring appeared at the most downfield. The signal at 152 ppm was due to the quaternary carbon C7 of the phenyl ring. The intense peak at 150 ppm referred to the quaternary carbon C4. The signals of carbon C6 occurred at a lower field than that of other methine carbons because it is located next to the nitrogen atoms. The carbon signals at 123 and 129 ppm were attributed to the two equivalent carbon C8 and C9. The signals of carbon C10, C3, and C5 appeared at 116, 132, and 126 ppm, respectively. The signal carbon of CH_3 (C11) appeared at the highest field 21 ppm The ^{13}C NMR signals assignments were based on the ^{1}H-^{13}C HMQC NMR spectrum (Figure 20), which exhibited a correlation between ^{1}H NMR spectrum and ^{13}C NMR spectrum.

Nuclear Magnetic Resonance spectroscopy of the *ctc*-[Ru(4mazpy)$_2$Cl$_2$] complex

Table 10. ^{1}H and ^{13}C NMR spectroscopic data of the *ctc*-[Ru(4mazpy)$_2$Cl$_2$] complex

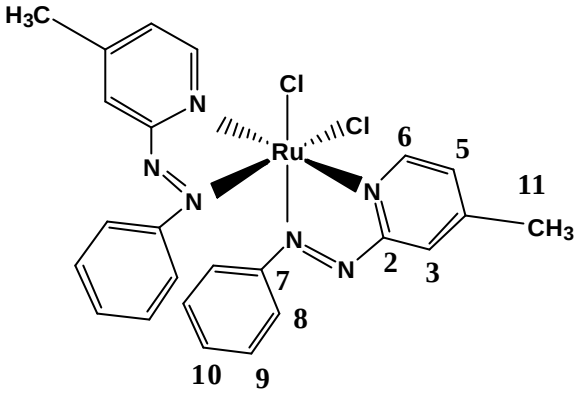

H-position	^{1}H NMR			^{13}C NMR
	? (ppm)	*J* (Hz)	Number of H	*?* (ppm)
6	9.17 (d)	6	1	150
3	8.32 (s)	-	1	127
5	7.31 (d)	5.4	1	126
10	7.27 (t)	7	1	130
9	7.11 (t)	7	2	128
8	6.84 (d)	7	2	122
11	2.65(s)	-	3	21
Quaternary carbons				166, C2 155, C7 149, C4

s = singlet, d = doublet, t = triplet

The ^{1}H NMR spectrum of the *ctc*-[Ru(4mazpy)$_2$Cl$_2$] complex showed only one set of protons similar to the free ligand. This result indicated that the complex was a symmetric molecule (C_2-symmetry). Moreover, the individual protons in the molecule showed different chemical shifts. The ^{1}H NMR spectrum of the *ctc*-[Ru(4mazpy)$_2$Cl$_2$] showed seven signals (Figure 21). It is interesting to note that the spectrum of the complex was divided into two parts (Table 10). The downfield portion was due to the pyridine protons (H3, H5, H6) and the upfield signals referred to azophenyl protons (H8, H9, H10). The most down field signal was assigned to H6. This is because of the influence of nitrogen atoms in the pyridine ring. The singlet peak at the highest field was referred to H11 which appeared at the lower field than the free ligand. It was due to the effect of the coordination with ruthenium metal. The signal of proton H6 in the pyridine rings occurred at the lowest field due to the influence of coordinated nitrogen atoms. The doublet peak at 7.31 ppm was assigned to the signals of proton H5. The triplet peak of proton H9 was observed at 7.11 ppm. It was splitted by proton H9 and H10 (J = 7 Hz).

The ^{13}C NMR of *ctc*-[Ru(4mazpy)$_2$Cl$_2$] is shown in Figure 23. The result of spectrum corresponded to the DEPT NMR spectrum (Figure 24). This trend is also found in free ligand. However, in complex, each signal slightly shifted to lower field or higher field than free ligand. The downfield signals at 166 ppm, 155 ppm, and 149 ppm were assigned to three quaternary carbons C2, C7, and C4, respectively. The carbon C6 signal occurred at 150 ppm, which was a lower field than for carbon C3 and C5. It was due to the effect of the nitrogen atoms. Moreover, the ^{13}C NMR signals assignment were based on the ^{1}H-^{13}C HMQC spectrum (Figure 25).

Nuclear Magnetic Resonance spectroscopy of the *ccc*-[Ru(4mazpy)$_2$Cl$_2$] complex

Table 11. ^{1}H and ^{13}C NMR spectroscopic data of the *ccc*-[Ru(4mazpy)$_2$Cl$_2$] complex

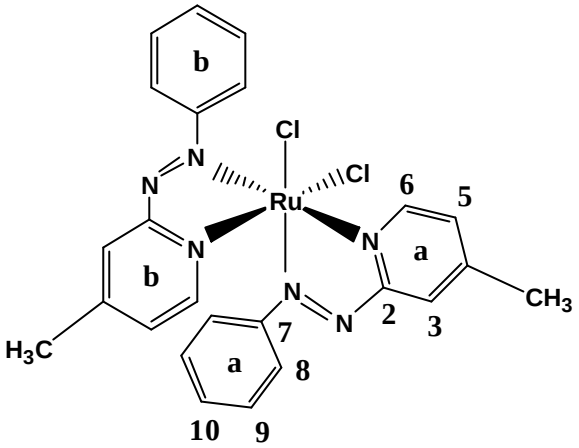

H-position	^{1}H NMR			^{13}C NMR
	? (ppm)	*J* (Hz)	Number of H	*?* (ppm)
6 (a)	9.56 (d)	6	1	149
3 (a)	8.32 (s)	-	1	124
3 (b)	8.22 (s)	-	1	126
8 (a)	7.77 (dd)	8.5, 2	2	125
5 (a)	7.65 (d)	4.5	1	125
10 (a)	7.45 (t)	7,7	1	131
9 (a)	7.36 (m)	-	2	127
10 (b)	7.34 (m)	-	1	129
9 (b)	7.18 (t t)	7.5, 8, 1.5	2	128
5,6 (b)	7.07 (m)	-	2	5a 125 5b 126 6b 147

Table 11. (Continued)

H-position	^{1}H NMR			^{13}C NMR
	? (ppm)	*J* (Hz)	Number of H	? (ppm)
8 (b)	6.69 (d of d)	8.5, 1.5	2	121
11 (a)	2.76 (s)	-	3	21
11 (b)	2.57 (s)	-	3	21
Quaternary carbons				2a 166 2b 165 7a 157 7b 155 4a 151 4b 150

s = singlet, d = doublet, t = triplet

The *ccc*-[Ru(4mazpy)$_2$Cl$_2$] is C_1-symmetrical and is expected to exhibit two sets of protons (Figure 26). This is indeed observed. The spectra showed that the pyridine protons are mostly affected when compared to the phenyl protons. The H6(A) and H3(A, B) signals are shifted downfield by approx. 1 ppm while, H9(A, B) and H10(A, B) are shifted upfield from those of the free ligand. Because the greater p-backbonding interaction to azo group will increase the electron density in the phenyl ring, this provided higher field phenyl protons. The pyridine protons H6(A) and H6(B) were observed at different chemical shifts. The proton H6 in pyridine ring A appeared at the lower field than pyridine ring B because it was trans to the N=N withdrawing group while proton H6 in pyridine ring B was trans to Cl. In addition, the proton signals in –CH_3 , ring A and ring B, showed the same effect of the trans

withdrawing group. The proton H8(B) was observed at the highest field of aromatic protons. The assignments of ^{1}H NMR were confirmed by using the ^{1}H-^{1}H COSY NMR spectrum (Figure 27).

The ^{13}C NMR spectrum is shown in Figure 28. The carbon signals of C5(A) and C8(A) occurred at the same chemical shift but can be assigned by ^{1}H-^{13}C HMQC spectrum. The DEPT spectral data (Figure 29) showed only signals of methine carbons and supported the ^{13}C NMR result.

Nuclear Magnetic Resonance spectroscopy of the *tcc*-[Ru(4mazpy)$_2$Cl$_2$] complex

Table 12. ^{1}H and ^{13}C NMR spectroscopic data of the *tcc*-[Ru(4mazpy)$_2$Cl$_2$] complex

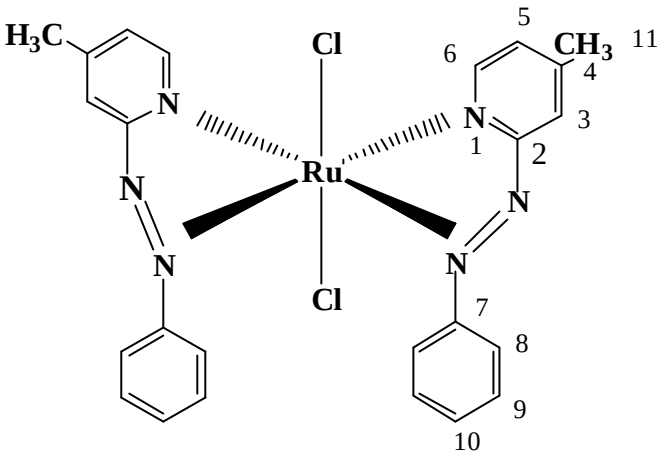

H-position	^{1}H NMR			^{13}C NMR
	? (ppm)	*J* (Hz)	Number of H	*?* (ppm)
6	8.75 (d)	5.5	1	148
3	8.40 (s)	-	1	125
5	7.59 (d)	5.5	1	124
8	7.52 (dd)	8, 1.5	2	122
10	7.17 (t)	7, 7	1	129
9	6.97 (t)	8.5	2	128
11	2.74 (s)	-	3	21
Quaternary carbons				166, C2 155, C7 153, C4

s = singlet, d = doublet, t = triplet, dd = doublet of doublet

The ^{1}H NMR spectrum of the *tcc*-[Ru(4mazpy)$_2$Cl$_2$] complex showed only one set of protons (Figure 31). This suggests that the complex contains the effective C_2-axis. Therefore both chelate rings in complex are magnetically equivalent at least on the NMR time scale. As was found for the *ctc*-[Ru(4mazpy)$_2$Cl$_2$], the spectrum of protons is clearly divided into two parts. The downfield portion is due to the pyridine protons(H6, H3, and H5) and the upfield signals refer to the phenyl protons. In addition, this complex was also studied by using simple correlation 1H-1H COSY NMR spectroscopy (Figure 32).

The ^{13}C NMR spectrum is shown in Figure 33. The spectrum of a quarternary carbon in the *tcc*-[Ru(4mazpy)$_2$Cl$_2$] complex showed at the same trend as for the 4mazpy ligand. The results from the ^{1}H-^{13}C HMQC spectrum also supported the position of carbon signals. Furthermore, The purposed structure of the *trans* complex was confirmed by the solid state structure study.

3.2.6 Cyclic Voltammetry

Electrochemical properties of all the complexes were studied by cyclic voltammetry at a glassy carbon working electrode and were examined in dichloromethane using tetrabutylammonuim hexafluorophosphate (TBAH) as supporting electrolyte at the scan rate of 100 mV s^{-1}. Voltammetric data are given in Table 13 and selected voltammograms are shown in Figure 36 to 39. The voltammograms displayed $Ru^{III/II}$ couple at the positive side and ligand reductions at the negative side. The potentials were compared with the potential of a ferrocene couple.

In this experiment, different scan rates were used to check the couple or the redox reaction. The couple having almost equal anodic and cathodic current was referred to as a reversible couple. On the other hand, the unequal currents were referred to the unequally transfer of electron in reduction and oxidation. This led to an irreversible couple. When different scan rates were applied, these currents gave equal anodic and cathodic currents at higher scan rate, which led to quasi-reversible couple.

Table 13. Cyclic voltammetric[a] data for the 4mazpy ligand and the three complexes in 0.1 M TBAH dichloromethane at scan rate of 100 mV/s

Compound	$E_{1/2}$(V) (? E_p(mV))		
	Oxidation	Reduction	
4mazpy	-	-1.68 (94)	
ctc-[$Ru(4mazpy)_2Cl_2$]	0.66 (76)	-1.02 (80)	-1.54[b]
ccc-[$Ru(4mazpy)_2Cl_2$]	0.59 (82)	-1.16 (92)	-1.56[b]
tcc-[$Ru(4mazpy)_2Cl_2$]	0.45 (100)	-1.22 (115)	-1.69[b]

[a] $E_{1/2} = (E_{pa} + E_{pc})/2$, where E_{pa} and E_{pc} are anodic and cathodic peak potentials, respectively; ? $E_p = E_{pa} - E_{pc}$; [b]cathodic peak potential, V

In the potential range +0.5 to +1.5 V at a scan rate of 100 mV/s in dichloromethane, one electron oxidation response was observed corresponding to the Ru(II) ? Ru(III) couple. The oxidation process is shown in equation (1).

$$Ru(4mazpy)_2Cl_2 \quad ? \quad Ru(4mazpy)_2Cl_2^+ + e^- \qquad (1)$$

The data (Table 13) show that the *cis* complexes (*ctc* and *ccc*) exhibited higher potentials by 0.14-0.2 V than the *trans* (*tcc*) complex. In the *cis* isomers, the two azo functions are *cis*-oriented and p-backbonding interaction may lead to an increase in the effective charge on the ruthenium center and result in shift the ruthenium(III)/ruthenium(II) couple to more positive values than those for the *cis*-isomers. The *ctc* isomer showed a slightly higher Ru(III)/Ru(II) couple (0.07 V) than that of the *ccc* isomer. These were also supported by electronic spectral data.

In the potential range 0 to –2.0 V, reductive responses were observed under similar conditions using a glassy carbon working electrode. The reduction potentials were compared with the results from the free ligand. The free ligand showed one reversible two electron reduction responses with peak to peak separation at 94 mV, corresponding to the couple in equation (2).

$$4mazpy \overset{2e^-}{?} 4mazpy^{2-} \qquad (2)$$

The potential of this couple was –1.68 V, which was less positive than the azopyridine (-1.61 V) [Santra, *et al.*, 1999]. All the three complexes displayed one reversible, one electron reduction, and one irreversible peak of one electron.

Moreover, the reduction potential showed a positive shift from the free ligand value. The first reduction couple of the *ctc* complex (-1.02 V) occurred at a higher potential than that in the *ccc* (-1.16 V) and the *tcc* (-1.22 V.) complexes. These results showed that the *ctc* isomer accepted electron better than the other ones. In addition, it could be concluded that the 4mazpy ligand in *ctc* complex was more easily reduced than the other two complexes.

In comparison with the azpy complexes, the *ctc*-$Ru(azpy)_2Cl_2$ showed at the 0.71 V(Jullapan, T., 2004), the oxidation range which is more positive than that of *ctc*-$Ru(4mazpy)_2Cl_2$ (0.66 V). This showed that the azpy ligand can stabilzed the ruthenium(II) in the *ctc*-isomer more than in the 4mazpy ligand. The ?-acidity order of the ligands is as follows:

4mazpy ? azpy

In the $[Ru(4mazpy)_2Cl_2]$ complexes, the ability of 4mazpy ligand to stabilize the complex is as follow:

tcc ? ccc ? ctc

In addition, The results of voltammetry were supported by the electronic spectral data shown in Table 14.

7 DEC0H Comparison of electronic and redox properties of $[Ru(4mazpy)_2Cl_2]$ complexes

Properties	*ctc*-isomer	*ccc*-isomer	*tcc*-isomer
Ru(III)/Ru(II), $E_{1/2}$ (V)	0.66	0.59	0.45
MLCT band, $?_{max}$ (nm)	581	583	630

3.2.7 X-ray Crystallography

X-ray crystallography is the most important technique to identify the geometry of compounds. The single crystals of both *ctc*-[Ru(4mazpy)$_2$Cl$_2$] and *tcc*-[Ru(4mazpy)$_2$Cl$_2$] were grown to obtain the suitable X-ray quality crystals for structure determination. X-ray diffraction data were collected on the APEX CCD diffractometer with the SHELXTL NT (version 6.12) programs and equipped with graphite monochromatized Mo Ka radiation (? = 0.71073) at 293 K. The structures were refined by full-matrix least-squares on F^2. The structures of the two complexes, *ctc* and *ccc*, showed six coordination around the ruthenium atom.

(a) X-ray structure of *ctc*-[Ru(4mazpy)$_2$Cl$_2$]

The single crystal of *ctc*-[Ru(4mazpy)$_2$Cl$_2$] was obtained by slow diffusion of hexane into dichloromethane solution of the complex. The solid state structure of *ctc*-[Ru(4mazpy)$_2$Cl$_2$] is shown in Figure 40. The crystallographic data are shown in Table 15. Selected bond parameters associated with the metal ions are listed in Table 16.

Table 15. Crystallographic data of the *ctc*-[Ru(4mazpy)$_2$Cl$_2$] complex

Empirical formula	$C_{24}H_{22}Cl_2N_6Ru$
Formula weight	566.345
Temperature	293(2) K
Wavelength	0.71073 Å
Crystal system	Monoclinic
Space group	$P2_1/n$ (No. 14)
Unit cell dimensions	a = 9.2195(4) Å ? ?= 90^o
	b = 15.1113(7) Å ? = 90.6530(10)^o
	c = 17.0885(8) Å ? = 90^o
Volume	2380.59(19) Å ^{3}
Z	4
Density (calculated)	1.580 mg/m^3
Absorption coefficient	0.908 mm^{-1}
Goodness-of-fit on F^2	1.028
Final R indices [I>2sigma(I)]	*R1* = 0.0258, w*R2* = 0.0653
R indices (all data)	*R1* = 0.0300, w*R2* = 0.0675

Table 16. Selected bond lengths (Å) and angles (^{o}) for the *ctc*-[Ru(4mazpy)$_2$Cl$_2$] complex

Ru(1)-N(6)	1.9762(16)	Ru(1)-N(3)	1.9831(16)
Ru(1)-N(4)	2.0353(16)	Ru(1)-N(1)	2.0483(16)
Ru(1)-Cl(1)	2.3973(6)	Ru(1)-Cl(2)	2.3918(5)
N(2)-N(3)	1.284(2)	N(5)-N(6)	1.287(2)
N(6)-Ru(1)-N(3)	89.82(7)	N(6)-Ru(1)-Cl(2)	90.42(5)
N(6)-Ru(1)-N(4)	76.59(7)	N(3)-Ru(1)-Cl(2)	171.57(5)
N(3)-Ru(1)-N(4)	100.63(7)	N(4)-Ru(1)-Cl(2)	87.62 (5)
N(6)-Ru(1)-N(1)	101.04(7)	N(1)-Ru(1)-Cl(2)	95.26(5)
N(3)-Ru(1)-N(1)	76.43(7)	N(6)-Ru(1)-Cl(1)	170.97(5)
N(4)-Ru(1)-N(1)	176.32(6)	N(3)-Ru(1)-Cl(1)	90.29(5)
N(4)-Ru(1)-Cl(1)	94.51(5)	N(1)-Ru(1)-Cl(1)	87.76(5)
Cl(2)-Ru(1)-Cl(1)	90.79(2)		

The atomic arrangement around the ruthenium ion invokes sequentially two *cis*-chlorines, *trans*-N(pyridine), N and *cis*-N(azo), N' and corresponds to the *cis-trans-cis* configuration. The coordination around the ruthenium atom is distorted octahedron.

The chelate angles extended by 4-methyl-2-(phenylazo)pyridine were 76.59(7)^{o} and 76.43(7) ^{o} and deviate considerably from the ideal geometry (90 ^{o}). As a consequence of the constraint of the bite angle, the ligands are bent back from the coordinated chlorides. The *cis*-chloro angle of 90.79(2)^{o} is very nearly the ideal octahedral angle and is comparable to the reported values (Santra, *et al.*, 1999).

The N(4)-Ru(1)-N(1) angle is 176.32(6)° which is distorted from linearity by 3.68°. The *trans* angles around the ruthenium center in the planes range

from 170.97(5)° to 176.32(6)°, indicating distortion from rectilinear geometry. The N-N distances of 1.284(2) and 1.287(2) A°. The Ru-N(azo) distances (1.9762(16), 1.9831(16) A°) are shorter than those of Ru-N(pyridine) (2.0353(16), 2.0483(16) A°) and this is an indication of an M-L p–interaction that is localized in the M-azo fragment.

The two *trans*-pyridine rings are planar and makes an angle of 91.019(0.089) °. The two pendant phenyl rings are planar and intersect at an angle of 11.407(0.077) ° to each other. Two chelate planes deviat from orthogonality (dihedral angle 88.126(0.060)°) possibly due to steric interaction.

In comparison with the *ctc*-azpy complex [Seal, A., 1984], the Ru(II)-N(azo) bond lengths (average, 1.981 Å) are close to the bond distance in *ctc*-4mazpy complex. While, the N-N distances in the azpy complex (average 1.281 Å) are slightly different to those of the 4mazpy complex (average 1.286(2) Å).

(b) X-ray structure of *tcc*-[Ru(4mazpy)$_2$Cl$_2$]

The X-ray quality single crystal was grown by slow diffusion of dichlromethane solution of the complex *tcc*-[Ru(4mazpy)$_2$Cl$_2$] into acetonitrile. The structure of the *tcc* complex is shown in Figure 41. The crystallographic data are collected in Table 17 and the selected bond parameters are listed in Table 18.

Table 17. Crystallographic data of the *tcc*-[Ru(4mazpy)$_2$Cl$_2$] complex

Empirical formula	$C_{24}H_{22}Cl_2N_6Ru$
Formula weight	566.45
Temperature	293(2) K
Wavelength	0.71073 Å
&U WBDX WP	MonoFOLQF
Space group	P2(1) (No. 4)
Unit cell dimensions	a = 8.4492(14) Å ? = 90°
	b = 9.5028(15) Å ? = 102.785(2)°
	c = 15.299(3) Å ? = 90°
Volume	1197.9(3) Å^3
Z	2
Density (calculated)	1.570 mg/m^3
Absorption coefficient	0.902 mm^{-1}
Max. and min. transmission	0.940 and 0.745
Goodness-of-fit on F^2	0.888
Final R indices [I>2sigma(I)]	*R1* = 0.0293, w*R2* = 0.0448
R indices (all data)	*R1* = 0.0323, w*R2* = 0.0455

Table 18. Selected bond lengths (Å) and angles (^{o}) for the *tcc*-[Ru(4mazpy)$_2$Cl$_2$] complex

Ru(1)-N(6)	1.985(2)	Ru(1)-N(3)	1.994(3)
Ru(1)-N(4)	2.064(2)	Ru(1)-N(1)	2.097(3)
Ru(1)-Cl(2)	2.3674(9)	Ru(1)-Cl(1)	2.3931(9)
N(2)-N(3)	1.286(4)	N(5)-N(6)	1.300(3)
N(6)-Ru(1)-N(3)	105.77(10)	N(4)-Ru(1)-Cl(2)	87.85(7)
N(6)-Ru(1)-N(4)	76.04(10)	N(1)-Ru(1)-Cl(2)	86.73(8)
N(3)-Ru(1)-N(4)	176.63(11)	N(6)-Ru(1)-Cl(1)	97.56(7)
N(6)-Ru(1)-N(1)	173.04(11)	N(3)-Ru(1)-Cl(1)	88.72(7)
N(3)-Ru(1)-N(1)	75.63(11)	N(4)-Ru(1)-Cl(1)	88.22(7)
N(4)-Ru(1)-N(1)	102.93(11)	N(1)-Ru(1)-Cl(1)	89.26(8)
N(6)-Ru(1)-Cl(2)	86.35(7)	Cl(2)-Ru(1)-Cl(1)	173.63(4)
N(3)-Ru(1)-Cl(2)	95.07(7)		

Similar to the *ctc*-[Ru(4mazpy)$_2$Cl$_2$], the ruthenium ion of the *tcc*-[Ru(4mazpy)$_2$Cl$_2$] complex is six-coordinated, and the coordination geometry of ruthenium(II) is also a distorted octahedron. The chloride atoms occupy the *trans* positions. The two 4mazpy ligands bind the ruthenium ion through two pyridine-N and two azo-N atoms and correspond to the *trans-cis-cis* configuration.

The Cl(2)-Ru(1)-Cl(1) angle is 173.63(4)^{o} and is consistent with a distorted octahedral structure. The chelate bite angle of the N(4)-Ru(1)-N(1) is (75.89(7) ^{o}) close to the N(8)-Ru(1)-N(5) bite angle (75.40(7) ^{o}). The chelate ring, Ru(1), N(1), C(6), N(2), N(3), is planar and is similar to the other planarity of Ru(1), N(4),

C(18), N(5), N(6) and the interplanar angle is 10.32(0.11) ^{o}. The phenylazo plane makes an angle 66.84^{o} with the chelated azoimine fragment and suggests stereochemically nonequivalent C-H functions. Two *cis*-phenylazo planes are not parallel, and the dihedral angle is 7.44(0.16) ^{o}.

The Ru-N'[N(azo): N(3) or N(6)] bond length (average, 1.990(2) Å) is shorter than the Ru-N[N(pyridine): N(1) or N(4)] (average, 2.066(2) Å) bond distance by 0.076 Å. The shortening may be due to greater ?-backbonding, *d*(Ru)? ?*(azo). In this complex, the average N-N distance is 1.293(4) Å which is shorter than some reported values of free azo ligands [Ghosh, *et al.*, 1894] and essentially equivalent to that of *tcc*-[Ru(paiq)$_2$Cl$_2$] [Lu, *et al.*, 2003]. The coordination leads to a decrease in the N-N bond order due to both the ?-donor and ?-acceptor character of the ligand, the latter character having a more pronounced effect and possibly being the reason for elongation.